Rare Metal Materials and Engineering
Volume 50, Issue 10, October 2021
Available online at www.rmme.ac.cn

Science Press

Cite this article as: Song Zhiyuan, Li Xianrong, Zhuang Changwan, et al. Effect of Morphology of Amorphous TiO_2 Nanotube on Its Electrochemical Performance as Supercapacitors[J]. Rare Metal Materials and Engineering, 2021, 50(10): 3485-3494.

ARTICLE

Effect of Morphology of Amorphous TiO_2 Nanotube on Its Electrochemical Performance as Supercapacitors

Song Zhiyuan[1], Li Xianrong[1], Zhuang Changwan[1], Wei Aili[1], Zhang Wanggang[1], Liu Yi-ming[1,2]

[1] College of Materials Science and Engineering, Taiyuan University of Technology, Taiyuan 030024, China; [2] Shanxi Academy of Analytical Sciences, Taiyuan 030006, China

Abstract: Hydrogenated amorphous TiO_2 nanotube arrays (H@am-TNAs) with different tube diameter, length and wall thickness were prepared through the modified two-step electrochemical anodization and electrochemical hydrogenation method. Results show that the electrochemical hydrogenation has almost no effect on the topology of TiO_2 nanotube arrays. After electrochemical hydrogenation, the nanotubes have a specific capacitance of 4.05 $mF \cdot cm^{-2}$ at 100 $mV \cdot s^{-1}$ that is 20 times larger than that of the corresponding one without hydrogenation with the same tube length and diameter. The capacitance of the nanotube is not only related to the tube length but also influenced by tube diameter. The aspect ratio of the nanotubes shows a linear relationship if fitted by an exponential function. The areal capacitance/aspect ratio reaches 0.056, which is almost equivalent to that of the anatase phase TiO_2 nanotubes. The nanotubes anodized for 2 h own the smallest charge transfer resistance, the best ion diffusion/transportation kinetics, and the highest areal capacity. Furthermore, to study the wettability in the electrochemical properties of the H@am-TNAs, the same H@am-TNAs electrode was soaked in the electrolyte for different hours before *C-V* and *C-P* testing, and the results show that the capacitance decreases with increasing the soaking time.

Key words: supercapacitors; amorphous; titanium dioxides nanotubes; aspect ratio; electrochemical hydrogenation

Due to their fast charge/discharge capability, high power density and long-term cycling stability, supercapacitors (SCs) have been regarded as one of the most promising energy storage systems in addition to batteries[1, 2]. There are two different kinds of supercapacitors: the electrical double-layer capacitors (EDLCs) that usually rely on electrostatic charge dispersion and accumulation at the electrode-electrolyte interface, and the pseudocapacitors which are normally based on factors such as charge storage mechanism and active materials used[3-5]. In the electrical double-layer capacitors, carbon-based material is usually taken as the electrode owing to their advantages such as excellent conductivity and extraordinary chemical stability[6-9]. And EDLCs with carbon-based materials usually show lower capacitance than pseudocapacitors that rely on transition metal oxides, hydroxides, and conducting polymers[10-12].

Many factors, such as the morphologies, crystal structures and pore structures can influence the application of the SCs. However, the structure and the nature of the selected material are the main reasons influencing its electrochemical performance[13-16]. Among different materials that can be used as SCs, amorphous material have received increasingly more attention owing to its properties such as the disordered structure, and high chemical stability[17-19].

Recently, TiO_2 nanotube arrays (TNAs) have aroused extensive concern in rechargeable storage systems due to their ability to provide large specific surface area. Furthermore, the nanotubes prepared through the anodization of titanium sheets have a one-dimensional array structure, which provides a fast channel for electrons to reach the substrate through the nanotubes[20-22]. However, the poor electrical conductivity (10^{-5}~10^{-2} $S \cdot m^{-1}$) and low rate capability restrict its

Received date: October 17, 2020
Foundation item: Special Talents Science and Technology Innovation Project of Shanxi Province of China (201705D211007); Shanxi Provincial Natural Science Foundation of China (201801D121099, 201801D221140, 201903D421081)
Corresponding author: Zhang Wanggang, Ph. D., College of Materials Science and Engineering, Taiyuan University of Technology, Taiyuan 030024, P. R. China, E-mail: zwgang0117@163.com

application. Therefore, substantial improvement should be employed to enhance the conductivity of TiO_2 and strengthen the capacitive behavior and rate ability of electrode by altering the inherent performance of TiO_2.

Many methods were used to prepare the TiO_2 nanotubes, the most attractive of which is the anodic oxidation of Ti sheets inside F^- based electrolyte [23-26]. The length and diameter of the nanotube arrays can be adjusted through changing the electrolyte and anodization time[27-29]. And the nanotube dimensions and morphology mainly depend on the anodization conditions like electrolyte, anodization time, voltage and temperature[30]. The diameter and tube length can be varied by changing these anodization parameters. Although there are many researches about the TiO_2 nanotubes as the supercapacitors[31-34], most of them are focused on crystallized TiO_2. The information regarding the effect of the morphology of the amorphous nanotubes on their electrochemical performance is scare. In this study, amorphous TiO_2 nanotubes (am-TNAs) with different lengths and diameters were prepared, and then doped with H by electrochemical method (H@am-TNAs). The electrochemical performance of the H@am-TNAs was studied, and more importantly, the relationship between the electrochemical performance and the morphology (length and pore diameter) of the H@am-TNAs were built up. We show that there is an appropriate aspect ratio when the areal capacitance is maximum. The aim of this work is to explore the possibility of amorphous titanium oxide nanotubes as supercapacitors and the effects of the tube length and diameter on the electrochemical performance of the H@am-TNAs.

1 Experiment

1.1 Preparation of TiO_2 nanotubes

The preparation of TiO_2 nanotube arrays by two-step anodization has been reported in our pervious report[35]. In short, commercial Ti plates (30 mm×10 mm×0.1 mm, China Research Institute of Nonferrous Metals, China) were washed sequentially with acetone, alcohol and deionized water for 20 min, and then dried in air. The two-electrode structure was taken for anodization of the titanium plates. Pt was used as counter electrode and Ti was used as working electrode. The electrolyte was composed of 0.3 g NH_4F, 2 mL H_2O and 98 mL ethylene glycol. The constant voltage was 50 V. After anodized for 1 h at room temperature, the surface of TiO_2 nanotubes was cleaned by ultrasonic. Then the Ti sheet with a textured surface was anodized again for different time (0.5, 1, 1.5, 2, 3 h) under the same condition to produce relatively ordered TiO_2 nanotube arrays. The schematic diagram is shown in Fig.1a.

1.2 Preparation of hydrogenated TiO_2 nanotube arrays

Electrochemical hydrogenation doping of the TiO_2 nanotube arrays were conducted by the Wu's method[36], which was carried out in a two electrode cell. Pt was taken as anode and the prepared nanotube arrays were cathode in that two electrode cell. The electrochemical hydrogenation doping time was 30 s, the solution was 0.5 mol·L^{-1} Na_2SO_4 and the applied voltage was 5 V. The process of electrochemical hydrogenation was essentially electrolysis of water, which was already reported by Wu and coworkers[36], and during the doping process, many O_2 and H_2 bubbles can be seen on the outer surface of the Pt foil and the TiO_2 nanotubes. After the doping process, the color of the nanotubes changes from gray to black, as shown in Fig.1b, indicating that the hydrogen doping is successful. Some other researches[37, 38] also observed the same phenomenon, and they attribute the color change of the nanotube arrays to the increased defect density.

1.3 Characterization

The samples were observed by scanning electron microscope (SEM, TESCAN Mira3 LMH) at 10kV. The crystal phases of products were obtained by X-ray diffraction (XRD, Rigaku SmartLab) with Cu Kα radiation from 20° to 80°. The binding energy and chemical states were examined using X-ray photoelectron spectroscopy (XPS, Escalab 250).

1.4 Measurements of electrochemical performance

Autolab (PGSTAT302N, Metrohm) was served as electrochemical measurements. The electrolyte was 0.5 mol·L^{-1} Na_2SO_4 aqueous solution. Pt sheet was used as the counter electrode. Ag/AgCl electrode was taken as the reference electrode. The sample acted as the working electrode. The cyclic voltammetry was tested in a potential range of −0.3~0.6 V (vs. Ag/AgCl) at different scanning rates (50~1000 mV·s^{-1}). The galvanostatic charge-discharge (GCD) tests were conducted at different current densities from 25 μA·cm^{-2} up to 500 μA·cm^{-2} between − 0.3 and 0.6 V. Electrochemical

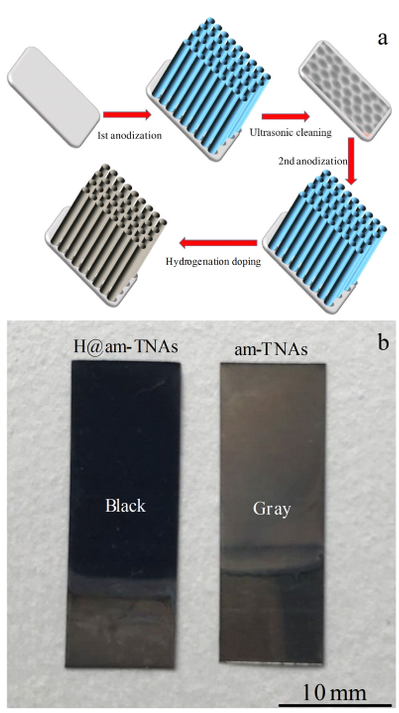

Fig. 1 Schematic diagram H@am-TNAs (a) and optical images of the anodized TiO_2 sheets with and without electrochemical hydrogenation (b)

impedance spectroscopy (EIS) was performed in a frequency range of 1 mHz to 100 kHz.

2 Results and Discussion

Fig. 2 depicts the XRD patterns of hydrogenated TiO_2 nanotube arrays. There are peaks at 38.4°, 40.2°, 53.0°, 63.0°, 70.7° and 76.3° corresponding to the (002), (101), (102), (110), (103) and (112) planes of Ti substrate, respectively. There are no peaks related to rutile and anatase TiO_2, confirming that the hydrogenated TiO_2 nanotube arrays are amorphous.

Fig.3a~3e show the surface and cross-section morphologies of the TiO_2 electrodes anodized for different hours. It is apparent that all of the electrodes are tubular structure. The tube diameter and tube length increase from ~52 nm to ~89 nm and from ~4.82 μm to ~12.41 μm, respectively when prolonging the anodization time from 0.5 h to 3 h. The longer anodization time leads to larger tube diameter and longer tube length. Fig. 3f summarizes the relationship between tube length/diameter and the anodization time. The length of the nanotubes linearly increases with the increase of the anodization time. However, the tube diameter reaches the maximum of ~89 nm, then decreases to ~82 nm when further prolonging the anodization time to 3 h.

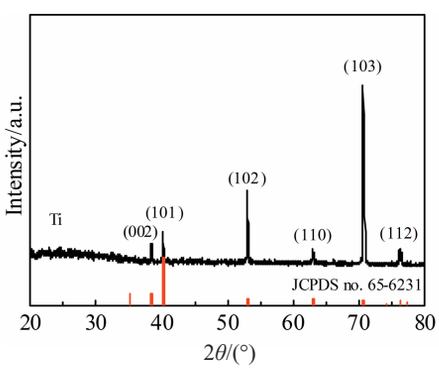

Fig.2 XRD patterns of H@am-TNAs

Fig.4a shows the XPS full spectrum of H@am-TNAs-1 and pristine am-TNAs-1. It can be seen that Ti and O are the main elements of the TNAs-1 electrodes before and after hydrogenation. Besides Ti and O elements, C and F can also be detected, which come from external pollution and the residue of the electrolyte during the anodization process, respectively. Fig. 4b shows the Ti 2p high-resolution XPS spectra of the two electrodes. The peaks located at 458.9 and 464.6 eV correspond to Ti^{4+} 3/2p and Ti^{4+} 1/2p for the pristine am-TNAs-1 electrode, respectively. After hydrogenation, however, there is a slightly positive shift (~0.02 eV) for the Ti 2p peak, which may be assigned to the changes in the electronic structure during the hydrogenation. The fitted two peaks centered at 458.8 and 464.5 eV correspond to Ti^{3+} 3/2p and Ti^{3+} 1/2p, respectively, indicating that part of Ti^{4+} in TiO_2 is reduced to Ti^{3+} after hydrogenation, because the hydrogenation process introduces oxygen vacancies (Vo) in the TiO_2 lattice. And after Vo is introduced, Vo will transfer two extra electrons to two Ti^{4+} ions to form Ti^{3+}. So the co-existence of Ti^{4+} and Ti^{3+} is also one of the criteria for determining the hydrogenation of TiO_2[39]. After hydrogenation, there will be an extra free electron at the 3d of Ti, which makes the carrier concentration inside TiO_2 increase significantly. According to

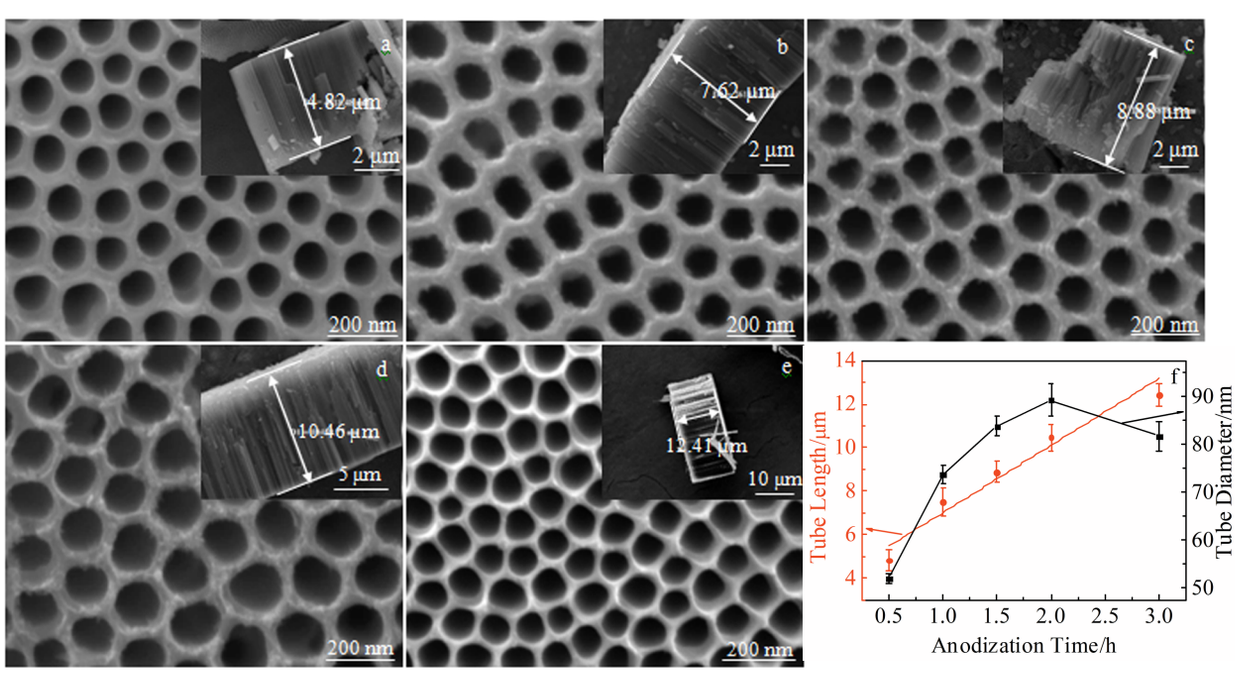

Fig.3 Surface and cross-section morphologies of the electrodes anodized for different time: (a) 0.5 h, (b) 1 h, (c) 1.5 h, (d) 2 h, and (e) 3 h; (f) relation of tube length/tube diameter vs anodization time

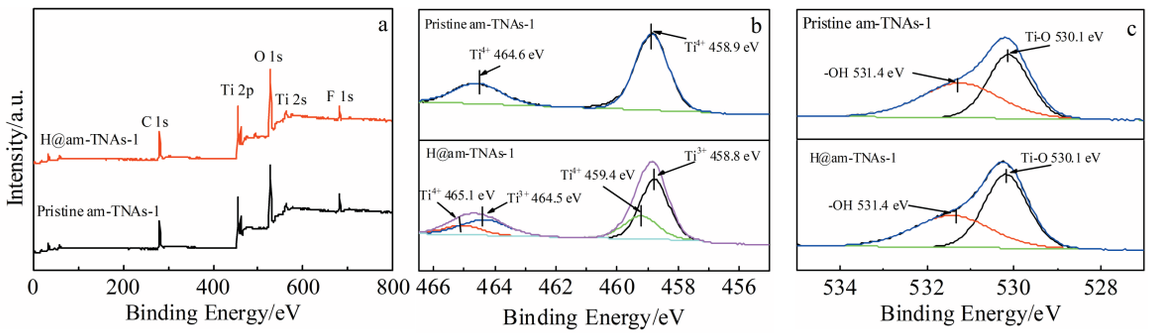

Fig.4 XPS spectra of pristine am-TNAs-1 and H@am-TNAs-1: (a) survey spectra, (b) Ti 2p core level high resolution spectra, and (c) O 1s core level spectra

Boltzmann's theory, the conductivity of semiconductor materials is directly proportional to the carrier concentration[40]. Therefore, the conductivity of TiO_2 can be significantly improved by hydrogenation. Fig. 4c shows the high-resolution XPS spectra of O 1s. There is no obvious change before and after hydrogenation. The peaks at 530.1 and 531.4 eV correspond to Ti-O bonds and -OH groups, respectively.

The electrochemical performance of these samples were investigated by GCD tests, which is shown in Fig. 5. Fig. 5a shows the GCD curves for pristine TiO_2 nanotube arrays electrode after anodization for 1 h (pristine am-TNAs-1) under the current density 0.025 and 0.1 $mA·cm^{-2}$. It can be seen that the GCD curves of the electrodes have nearly triangular shape, which means that the TiO_2 electrodes have the typical double-layer capacitor characteristic[41]. Fig. 5b exhibits the GCD curves of the TiO_2 nanotube array electrodes under the same anodization parameter before and after hydrogenation at the same current density (25 $\mu A·cm^{-2}$). It is apparent that the nanotubes after hydrogenation have longer discharge duration compared with pristine TiO_2 under the same current density, and such a trend reveals the important role of hydrogenation in improving the electrochemical performance of the supercapacitors made of TiO_2 nanotubes. Actually, the areal capacitance of the H@am-TNAs-1 tested at 25 $\mu A·cm^{-2}$ is almost 4 times larger than that of pristine am-TNAs-1. It has been reported that the Ti^{3+}, -OH groups and oxygen vacancies can be generated in the hydrogenation of TiO_2 nanotube, which decreases the band gap and improves the conductivity of TiO_2[42]. The improved conductivity may be the main reason

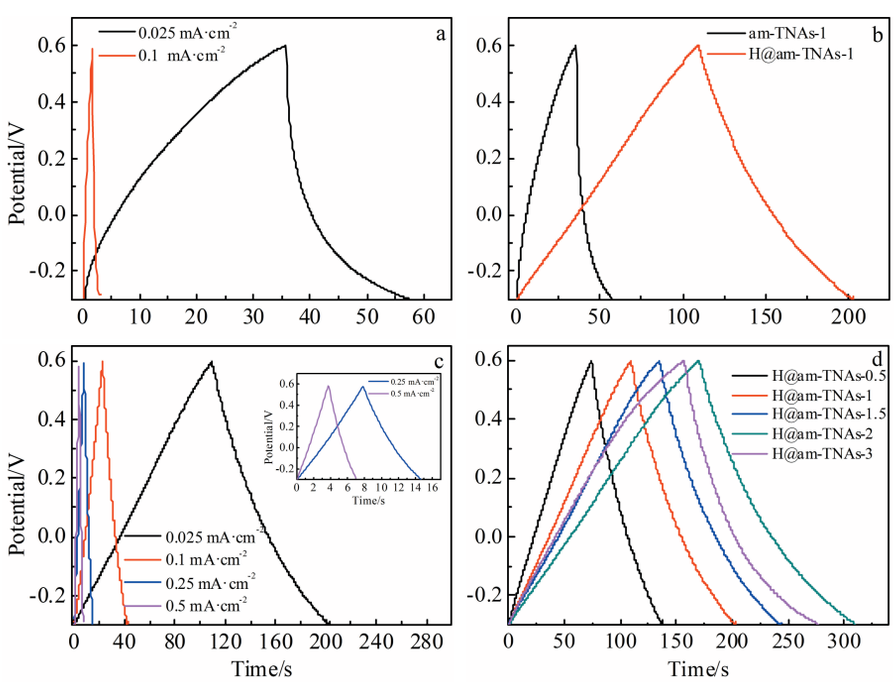

Fig. 5 Charge-discharge curves of pristine am-TNAs-1 and H@am-TNAs: (a) pristine am-TNAs-1 anodized for 1 h collected at 0.025 and 0.1 $mA·cm^{-2}$, (b) H@am-TNAs-1 and am-TNAs-1 with the same tube parameter collected at 0.025 $mA·cm^{-2}$, (c) H@am-TNAs-1 collected at different current densities, and (d) H@am-TNAs with different parameters collected at 0.025 $mA·cm^{-2}$

for the better storage of charges of H@am-TNAs-1.

It is well know that the small electrical conductivity of TiO_2 forms the current resistance (*I-R*) drop[43]. And the following equation can be used to calculate the *I-R* drop[44, 45]:

$$R = \frac{V_{charge} - V_{discharge}}{2I} \quad (1)$$

where V_{charge} is the voltage of the cell at the end charge, $V_{discharge}$ is the voltage of the cell at the starting discharge and I is the absolute value of the charge/discharge current.

This gives an average value of 21 and 1 Ω for the pristine and H doped nanotube array electrodes with the same tube length and diameter. Since there is a close relationship between *I-R* drop and charge-transfer resistance (R_{ct}), if the *I-R* drop is compared to the capacitance, the capacitance and discharge time show an opposite trend compared with the *I-R* drop. In other words, the *I-R* drop decreases, and the capacitance and discharge time increase. Therefore, the lower *I-R* drop generates better electrochemical properties[43].

Fig.5c depicts the GCD curves of H@am-TNAs-1 collected under diverse current densities. And it is apparent that the areal capacitance of H@am-TNAs-1 gradually reduces with increasing charge-discharge current densities, because the ion accessibility is limited in the inner region of the porous structure on the relevant timescale[46]. Fig. 5d compares the charge-discharge properties of H@am-TNAs with different parameters under 25 μA·cm^{-2}, and we can see that to some extent, the longer tube length and bigger tube diameter lead to better areal capacitance, meaning that the capacitance is related to morphology.

The average specific capacitance is estimated to be 1.45 mF·cm^{-2} for pristine am-TNAs-1, 3.23 mF·cm^{-2} for H@am-TNAs-0.5, 4.17 mF·cm^{-2} for H@am-TNAs-1, 4.94 mF·cm^{-2} for H@am-TNAs-1.5, 6.52 mF·cm^{-2} for H@am-TNAs-2 and 6.17 mF·cm^{-2} for H@am-TNAs-3, obtained by the following equation[47]:

$$C = \frac{2i_m \int V\mathrm{d}t}{V^2 \Big|_{V_i}^{V_f}} \quad (2)$$

where C (mF·cm^{-2}) represents the GCD specific capacitance; i_m (mA·cm^{-2}) is the charge/discharge current density; $\int V\mathrm{d}t$ is the integral area surrounded by charge/discharge curve and x axis; V_i and V_f are the potential with initial and final values of V, respectively.

In order to further study the impact of H-doping on the electrochemical performance of amorphous TiO_2 nanotube arrays, the cyclic voltammetry test was carried out in a traditional three-electrode cell in 0.5 mol·L^{-1} Na_2SO_4 aqueous solution. Fig. 6a shows the *C-V* curves of the same morphology amorphous TiO_2 nanotube array electrodes at the scanning rate of 100 mV·s^{-1} before and after H doping. Obviously, the cyclic voltammetry curve of H@am-TNAs-1 shows a larger integral area and current response than that of original TiO_2 electrodes, suggesting a distinctly improved capacitance behavior. Moreover, this *C-V* curves of H@am-TNAs-1 electrode present a nearly rectangular shape, indicating great charge transmission and small contact resistance on electrodes[20,48]. Furthermore, the rectangular *C-V* responses at 100 mV·s^{-1} for the H@am-TNAs-1 suggest an ideal capacitive behavior revealing fast diffusion of ions

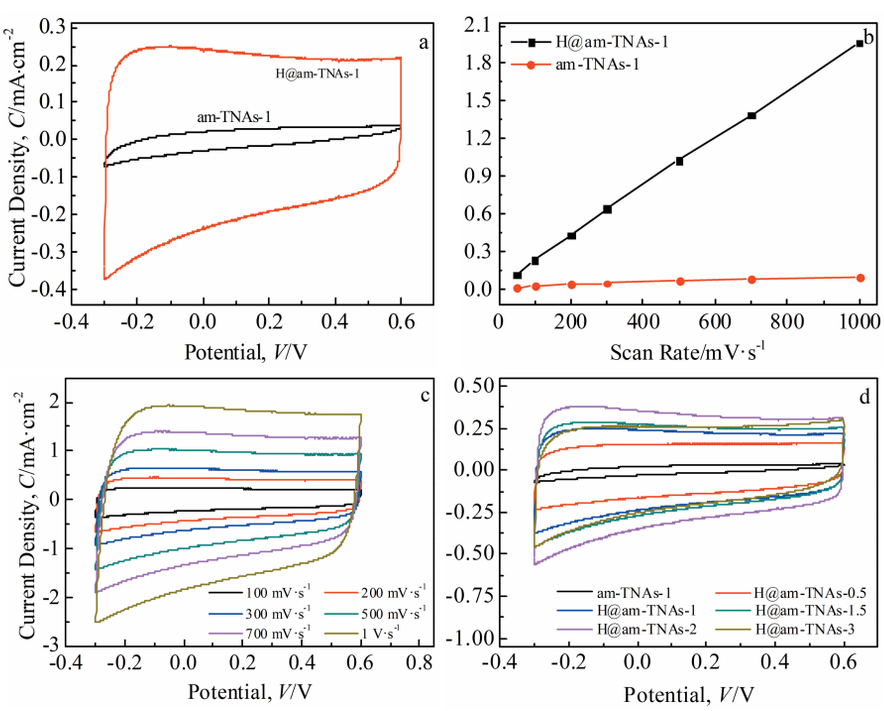

Fig.6 *C-V* curves of the samples: (a) am-TNAs and H@am-TNAs electrodes at a scan rate of 100 mV·s^{-1}; (b) current density as a function of scan rate for am-TNAs and H@am-TNAs electrodes; (c) H@am-TNAs-1 electrode recorded at different scan rates from 100 mV·s^{-1} to 1 V·s^{-1}; (d) am-TNAs-1 and H@am-TNAs electrodes with different tube lengths and diameters at scan rates of 100 mV·s^{-1}

throughout the device, including the TiO_2 nanotube array channels, and a very rapid current response to voltage reversal[49]. The ratio of the area at cathodic scan to that at anodic scan exams the coulombic efficiency and is found to be 91.2% and 95.6% for pristine am-TNAs electrode and H@am-TNAs-1 electrode with the same tube length and tube diameter, respectively under the scanning rate of 100 $mV \cdot s^{-1}$. The larger resistance at more positive potential of that electrode results in the decreased current density owing to this n-type semiconductor performance of titanium dioxide nanotube arrays[20,50].

Fig. 6b shows the current density of pristine am-TNAs-1 and H@am-TNAs-1 electrodes as a function of scan rate. The current densities increase with the increase of potential scanning rate, indicating an excellent rate property and great capacitive behavior of H@am-TNAs-1 electrode. Moreover, the comparatively linear increase of the current density with increasing scan rate suggests that the charge is primarily non-faradic in nature and the contribution of the faradic part might be very little, if it exists[31,51].

Furthermore, when the scan rate increases from 0.1 $V \cdot s^{-1}$ to 1 $V \cdot s^{-1}$, all the cyclic voltammetry curves of the H@am-TNAs-1 exhibit unaltered rectangular shapes (Fig. 6c), indicating the excellent capacitance behavior and high rate capability. Fig. 6d compares the *C-V* curves of the H@am-TNAs nanotubes with different lengths and diameters. As expected and consistent with the charge-discharge curves in Fig. 5d, the longer tube length and bigger tube diameter lead to better areal capacitance, further indicating that the capacitance is related to morphology.

The capacitance of the electrode can be calculated through the following equation[52]:

$$C = \frac{1}{SvV}\int I(V)\,\mathrm{d}V \tag{3}$$

where C ($F \cdot cm^{-2}$) represents the capacitance; S (cm^2) is the surface area of active material; v ($V \cdot s^{-1}$) is the scanning rate; ΔV (V) is the potential voltage range; I (A) represents the current.

Fig. 7 shows the calculated capacitance of pristine am-TNAs-1 and H@am-TNAs electrodes. It is apparent that when the scanning rate increases, the capacitance of these electrodes decreases. The reason for this may be the restricted dispersion of ions in these nanotubes[53, 54]. Since the diffusion of ions from the electrolyte requires more time to permeate deeper into the pores, leading to more effective ion permeation into the open-pore structure and consequently higher capacitance. So the areal capacitance of the pristine am-TNAs-1 electrode at lower scan rates is much greater than at higher scan rates[49]. All of the H@am-TNAs electrodes have much higher capacitance than pristine am-TNAs-1. As expected, the H@am-TNAs-2 possesses the highest specific capacity (6.0 $mF \cdot cm^{-2}$ at 50 $mV \cdot s^{-1}$). Because the longer anodization time not only leads to longer tube length but also bigger tube diameter. As the anodization time increases from 0.5 h to 2 h, the capacitance increases. However, when further prolonging the anodization time to 3 h, the capacitance decreases a little. From Fig. 3f, we know that though the tube length increases with the increase of the anodization time, the tube diameter decreases.

And for the pristine am-TNAs-1 and H@am-TNAs-1 electrodes with the same tube length and diameter, the specific capacitance of H@am-TNAs-1 electrodes is 4.05 $mF \cdot cm^{-2}$, which is 20 times larger than that of pristine am-TNAs-1. Furthermore, when the scan rate increases from 50 $mV \cdot s^{-1}$ to 1 $V \cdot s^{-1}$, the capacitance of the H@am-TNAs-0.5, H@am-TNAs-1, H@am-TNAs-1.5, H@am-TNAs-2 and H@am-TNAs-3 electrodes keeps high retentions of 65.0%, 69.5%, 66.9%, 69.0% and 66%, respectively. However, for the pristine am-TNAs-1 electrode, the high rate capacitance keeps only 33% as the scan rate increases from 50 $mV \cdot s^{-1}$ to 1 $V \cdot s^{-1}$.

From above analysis we know that the capacity of the H@am-TNAs electrode is closely related to its morphology. To find the relation between the capacitance and the morphology, it is necessary to make the morphology of the electrodes dimensionless. If we divide the capacity of the electrode by its corresponding aspect ratio (length/diameter), we get the relationship between the areal capacitance/aspect ratio and the anodization time, which is shown in Fig. 8. Fig. 8a shows the relationship between the anodization time and aspect ratio fited by exponential function. And Fig. 8b shows the relationship between the anodization time and areal capacitance/aspect ratio. As expected, the nanotubes after anodization for

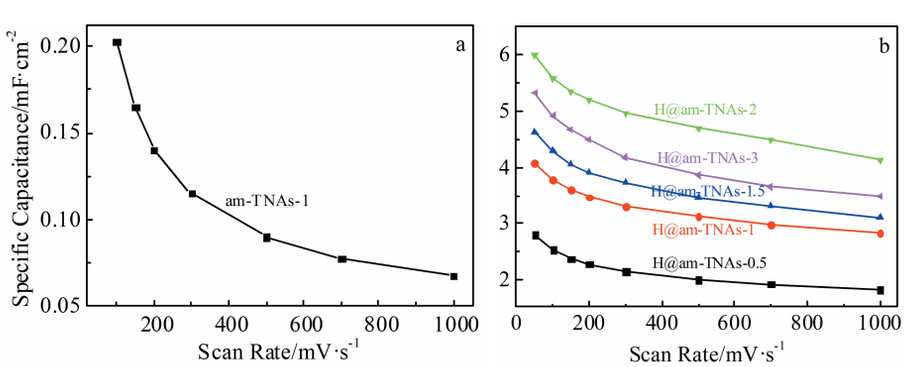

Fig.7 Calculated capacitance of pristine am-TNAs-1 (a) and H@am-TNAs (b) electrodes as a function of scan rate

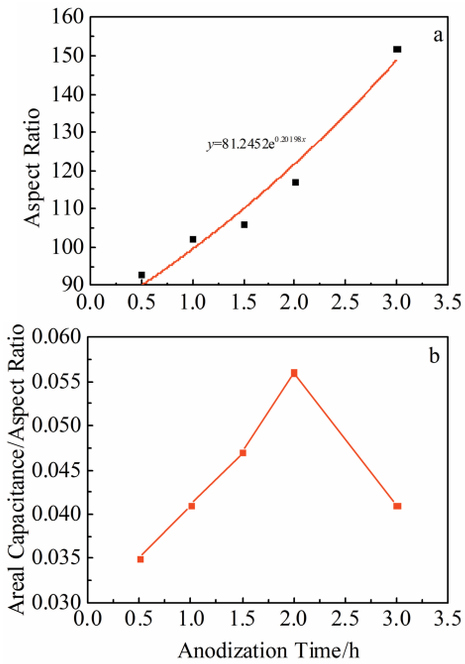

Fig.8 Anodization time vs aspect ratio (a) and areal capacitance/aspect ratio (b)

2 h own the highest areal capacitance/aspect ratio.

Table 1 summarizes the areal capacitance of H doped TiO_2 nanotube arrays as SCs after making electrodes morphology dimensionless. One has to note that since little work focused on amorphous TiO_2, the amorphous phase is compared with the crystallized anatase phase. It can be seen that the areal capacitance/aspect ratio obtained for amorphous TiO_2 is almost equivalent to that of anatase phase, which is 0.056.

Electrochemical impedance spectroscopy is widely used to study porous electrodes. It gives a good understanding regarding the internal resistance of the electrode material and the resistance between the electrode and the electrolyte[57,58]. Fig. 9a shows the Nyquist plots of the 6 working electrodes with different length and diameters, with EIS carried out and analyzed in the frequency range of 100 kHz to 1 mHz. It is apparent that the impedance diagrams for all of H@am-TNAs electrodes exhibit practically vertical line that represents ideal capacitive behavior. However, for amorphous TiO_2 nanotube array electrode without hydrogenation, the Nyquist plot bends down to the real axis, indicating an inferior capacitor characteristics. During the electrochemical hydrogenation process, lots of bubble, which are oxygen and hydrogen, can be observed. And those generated hydrogen can react with TiO_2 to form Ti^{3+} and oxygen vacancies, which improve electronic conductivity of H@am-TNAs. The H@am-TNAs possesses large power characteristics and excellent double-layer capacitive behavior. All of these changes increase the accumulation of electrolyte ions at the interface between electrolyte and TiO_2, resulting in the increase of the storage of charges in H@am-TNAs.

The equivalent circuit model (Fig. 9b) is fitted with the experimental data of impedance spectrum for better quantitative analysis. The equivalent circuit consists of the resistance of the electrolyte, R_s, whereas the values are similar because of the use of identical electrolyte system, the solution resistance R_1, contact resistance R_2 between electrolyte and electrodes, one constant phase element of CPE_1 standing for the structure of electric double-layer capacitance, and another

Table 1 Comparison of the results of some H doped TiO_2 nanotube arrays in the literature

Crystal structure	Aspect ratio	Areal capacitance /mF·cm^{-2}	Areal capacitance/ aspect ratio	Electrolyte		Ref.
				Na_2SO_4 content/ mol·L^{-1}	Current density or scan rate	
Anatase	23~40	1.84	0.046~0.08	0.5	50 μA·cm^{-2}	[55]
Anatase	250	20.08	0.08	0.5	50 μA·cm^{-2}	[36]
Anatase	16	3.24	0.2	0.5	100 mV·s^{-1}	[56]
Amorphous	116	6.52	0.056	0.5	25 μA·cm^{-2}	This work

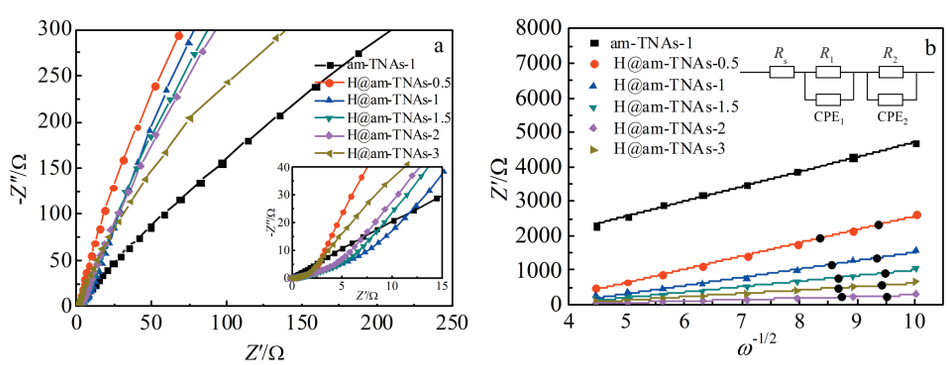

Fig.9 Nyquist plots (a) and Z' vs $w^{-1/2}$ (b) for pristine am-TNAs and H@am-TNAs electrodes

constant phase element of CPE_2 representing the capacitance from the internal structure of the electrochemical cell, which were calculated using the equivalent circuit in Table 2. R_2 value of the pristine am-TNAs sample (295.4 Ω) decreases dramatically to 31.86 Ω after H doping, suggesting that the electrochemical performance is enhanced by hydrogen doping. Additionally, from the relationship between Z' and $\omega^{-1/2}$ ($\omega=2\pi f$) in the low-frequency region, as shown in Fig.9b, compared with the electrodes without hydrogenation, the slope for all of the H@am-TNAs electrodes is lower, indicating smaller charge transfer resistance and better ion transportation kinetics and necessity of hydrogenation process[41]. The smallest charge transfer resistance for the H@am-TNAs-2 means the best ion diffusion/transportation kinetics, so it has the highest areal capacitance.

It is well known that for the am-TNAs electrodes, the electrochemical processes involve the migration and diffusion of ions in the nanotubes. A longer tube length means that the ions need more time to diffuse to the bottom part while smaller diameter will also impede the ion diffusion, so both longer tube length and smaller inner diameter lead to slower ion diffusion rate, which results in lower areal capacitance. So from this point of view, for the am-TNAs electrodes, the capacity performance is not only related to the length of the tube, but also closely related to diameter. And from the above analysis, we know that if both the two main factors of length and diameter are considered, there must be an optimal aspect ratio to ensure the fast ions diffusion and the best electrochemical performance. Based on our analysis, the best aspect ratio is ~120.

We know that the wettability between the electrolyte and the electrode is also vital to the electrochemical properties for the electrode. To study the wettability of H@am-TNAs-1, the same H@am-TNAs-1 electrode was soaked in the electrolyte for different time before *C-V* and *C-P* testing. Fig.10a presents the *C-V* curves of H@am-TNAs-1 electrode soaked in the Na_2SO_4 for different time under the scan rate of 100 $mV\cdot s^{-1}$, and Fig. 10b shows corresponding charge-discharge curves. It is apparent that capacitance of the H@am-TNAs-1 electrode decreases when the soaking time prolongs from 0 h to 24 h and is almost stable after 48 h soaking.

Fig. 10c shows the calculated capacitance of H@am-TNAs electrodes soaked in the electrolyte for different time as a function of scan rate. From the plots, we know that the samples without soaking show the best capacitance. The specific capacitance is nearly unchanged when the soaking time prolongs from 48 h to 72 h, meaning that the ion diffusion is almost saturated after the electrodes are soaked in the electrolyte for 48 h.

For high-performance supercapacitors, excellent cycling stability is one of the most critical and indispensable characteristics. Fig.11 shows the cycling performance for both pristine am-TNAs-1 and H@am-TNAs-1 electrodes under the scan rate of 100 $mV\cdot s^{-1}$ for 1200 cycles. As depicted in Fig.11, the 600th and 1200th cycles of pristine am-TNAs-1 and H@am-TNAs-1 electrodes are almost coincident, meaning that the capacitance of the electrodes is nearly stable after 600 cycles. And this can be further supported by the capacitance retention vs. cycle number curves in Fig. 11b and 11d. The capacitances of pristine am-TNAs-1 and H@am-TNAs-1

Table 2 Physicochemical properties measured and calculated from EIS spectra

Samples	R_s/Ω	R_2/Ω
Am-TNAs-1	3.019	295.4
H@am-TNAs-0.5	3.007	43.21
H@am-TNAs-1	2.878	31.86
H@am-TNAs-1.5	2.941	28.97
H@am-TNAs-2	2.913	16.46
H@am-TNAs-3	3.257	48.38

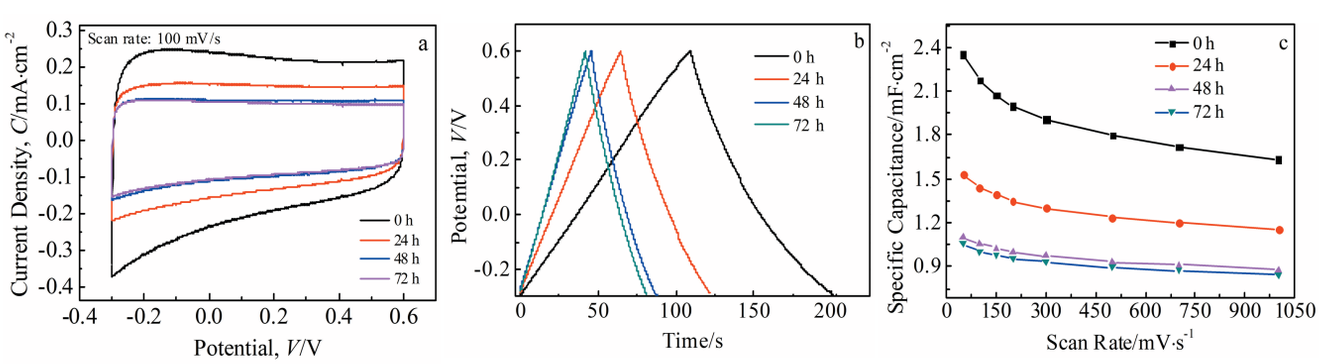

Fig.10 *C-V* curves (a), charge-discharge curves (b) and calculated capacitance (c) of H@am-TNAs-1 electrodes soaked in the electrolyte for different time

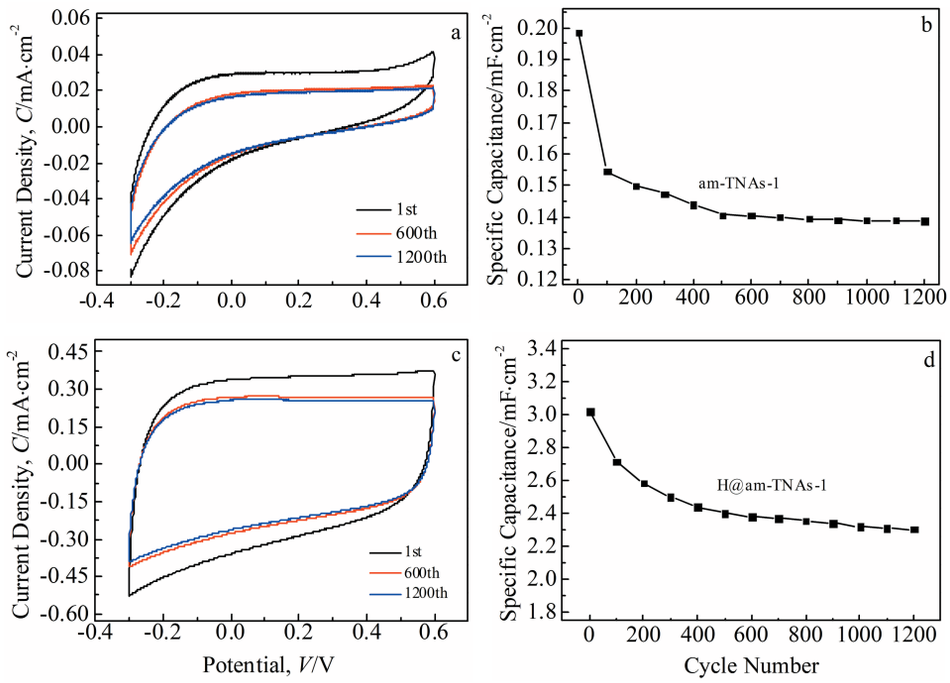

Fig.11 *C-V* curves (a, c) and capacitance retention vs cycle number curves of electrodes: (a, b) pristine am-TNAs-1 and (c, d) H@am-TNAs-1

electrodes drop by 30.3% and 23.5%, respectively after 1200 cycles.

3 Conclusions

1) The H@am-TNAs nanotube have a specific capacitance of 4.05 $mF \cdot cm^{-2}$ at a scan rate of 100 $mV \cdot s^{-1}$, which is 20 times larger than that of the corresponding one without hydrogenation with the same tube length and diameter.

2) The capacitance of the H@am-TNAs electrodes is related to morphology. The longer the tube length and the bigger the tube diameter, the better the areal capacitance.

3) All the H@am-TNAs electrodes have a smaller charge transfer resistance and the best ion diffusion/transportation kinetics.

4) When the optimal aspect ratio is about 120, the ion diffusion speed is the fastest and the electrochemical performance is the best. At this point, the areal capacitance/ aspect ratio of amorphous titanium dioxide is almost equal to that of anatase phase.

5) The same H@am-TNAs electrodes are immersed in the electrolyte for different time, and the specific capacitance decreases as the soaking time increases. The electrodes without soaking show the best capacitance.

References

1 Hai Z, Karbalaei Akbari M, Xue C *et al. Composites Communications*[J], 2017, 5: 31

2 He Chong, Chen Zhijie, Lin Deyuan *et al. Rare Metal Materials and Engineering*[J], 2017, 46(9): 2589 (in Chinese)

3 Zhou He, Zhang Yanrong. *The Journal of Physical Chemistry C* [J], 2014, 118(11): 5626

4 Simon P, Gogotsi Y. *Materials for Electrochemical Capacitors, Nature Materials*[J], 2008, 7(11): 845

5 Wang Ying, Wang Peng, Song Wenxue. *Rare Metal Materials and Engineering*[J], 2019, 48(3): 1022 (in Chinese)

6 Huang Yi, Liang Jiajie, Chen Yongsheng. *Small*[J], 2012, 8(12): 1805

7 Kiamahalleh M V, Zein S H S, Najafpour G *et al. Nano*[J], 2012, 7(2): 1 230 002

8 Tan C W, Tan H K, Ong Y T *et al. Environmental Chemistry Letters*[J], 2012, 10(3): 265

9 Pandolfo A G, Hollenkamp A F. *Journal of Power Sources*[J], 2006, 157(1):11

10 Jiang Jian, Li Yuanyuan, Liu Jinping *et al. Advanced Materials* [J], 2015, 24(38): 5166

11 Yan Jun, Wang Qian, Wei Tong *et al. Advanced Energy Materials* [J], 2014, 4(4): 157

12 Wang Rutao, Yan Xingbin, Lang Junwei *et al. Journal of Materials Chemistry A*[J], 2014, 2(32): 12 724

13 Li Bing, Zheng Mingbo, Xue Huaiguo *et al. Cheminform*[J], 2016, 3(2): 175

14 Pang Huan, Li Xinran, Zhao Qunxing *et al. Nano Energy*[J], 2017, 35: 138

15 Zhu Yanwu, Murali S, Stoller M D *et al. Science*[J], 2011, 332(6037): 1537

16 Chakravarty D, Kumar P, Ugale V S *et al. European Journal of Inorganic Chemistry*[J], 2015(9): 2544

17 Xiao Xiao, Li Xinran, Zheng Shasha *et al. Advanced Materials Interfaces*[J], 2017, 4(6): 1 600 798

18 Wang Yang, Ye Guiqin, Chen Huanhuan *et al. Journal of Materials Chemistry A*[J], 2015, 3(29): 15 292

19 Jabeen N, Hussain A, Xia Q *et al. Advanced Materials*[J], 2017, 29(32): 1 700 804

20 Shao Zhou, Li Hongji, Li Mingji *et al. Energy*[J], 2015, 87: 578
21 Gobal F, Faraji M. *Journal of Electroanalytical Chemistry*[J], 2013, 691: 51
22 Zhu Changrong, Xia Xinhui, Liu Jilei *et al. Nano Energy*[J], 2014, 4: 105
23 Macak J M, Albu S P, Schmuki P. *Rapid Research Letters*[J], 2010, 1(5): 181
24 Macak J M, Gong B G, Hueppe M *et al. Advanced Materials*[J], 2007, 19(19): 3027
25 Macak J M, Schmuki P. *Electrochimica Acta*[J], 2006, 52(3): 1258
26 Wei W, Berger S, Hauser C *et al. Electrochemistry Communications*[J], 2010, 12(9): 1184
27 Fang Haitao, Liu Min, Wang Dawei *et al. Nanotechnology*[J], 2009, 20(22): 225 701
28 Paulose M, Shankar K, Yoriya S *et al. The Journal of Physical Chemistry B*[J], 2006, 110(33): 16 179
29 Shankar K, Mor G K, Prakasam H E *et al. Nanotechnology*[J], 2007, 18(6): 65 707
30 De Tacconi N, Chenthamarakshan C, Yogeeswaran G *et al. The Journal of Physical Chemistry B*[J], 2006, 110(50): 25 347
31 Salari M, Aboutalebi S H, Konstantinov K *et al. Physical Chemistry Chemical Physics: PCCP*[J], 2011, 13(11): 5038
32 Qiu Jingxia, Li Sheng, Gray Evan *et al. Journal of Physical Chemistry C*[J], 2014, 118(17): 8824
33 Ramadoss A, Sang J K. *Journal of Alloys & Compounds*[J], 2013, 561: 262
34 Yu Cuiping, Wang Yan, Cui Jiewu *et al. Acta Physico-Chimica Sinica*[J], 2017, 33(10): 1944
35 Zhang Wanggang, Liu Yiming, Li Wenyi *et al. Applied Surface Science*[J], 2019, 476: 948
36 Wu Hui, Li Dongdong, Zhu Xufei *et al. Electrochimica Acta*[J], 2014, 116(116): 129
37 Chen Xiaobo, Liu Lei, Yu Peter *et al. Science*[J], 2011, 331(6018): 746
38 Naldoni A, Allieta M, Santangelo S *et al. Journal of the American Chemical Society*[J], 2012, 134(18): 7600
39 Liu Lei, Chen Xiaobo. *Chemical Reviews*[J], 2014, 114(19): 9890
40 Heersche H, Jarillo-Herrero P, Oostinga J *et al. Nature*[J], 2007, 446: 56
41 Yan J, Ren C E, Maleski K *et al. Advanced Functional Materials* [J], 2017, 27: 1 701 264
42 Wang Gongming, Wang Hanyu, Ling Yichuan *et al. Nano Letters* [J], 2011, 11(7): 3026
43 Choi H J, Kim J H, Kim H K *et al. Electrochimica Acta*[J], 2016, 208: 202
44 Luo Jiayan, Xia Yongyao. *Journal of Power Sources*[J], 2009, 186(1): 224
45 Lee S H, Lee S G, Yoon J R *et al*. *Journal of Power Sources*[J], 2015, 273: 839
46 Futaba D N, Hata K, Yamada T *et al. Nature Materials*[J], 2006, 5(12): 987
47 Mai L Q, Minhaskhan A, Tian X *et al. Nature Communications* [J], 2013, 4(1): 2923
48 Zhou Zhengping, Wu Xiangfa, Hou Haoqing. *RSC Advances*[J], 2014, 4(45): 23 622
49 Salari M, Aboutalebi S H, Ekladious I *et al. Advanced Materials Technologies*[J], 2017, 3(2): 1 700 194
50 Wu Hui, Li Dongdong, Zhu Xufei *et al. Electrochimica Acta*[J], 2014, 116: 129
51 Stoller M D, Park S, Zhu Y *et al. Nano Letters*[J], 2008, 8(10): 3498
52 Salari M, Konstantinov K, Liu H K. *Journal of Materials Chemistry*[J], 2011, 21(13): 5128
53 Salari M, Aboutalebi S H, Chidembo A T *et al. Physical Chemistry Chemical Physics: PCCP*[J], 2012, 14(14): 4770
54 Wang J, Polleux J, Lim J *et al. Journal of Physical Chemistry C* [J], 2007, 111(40): 14 925
55 Zhou He, Zhang Yanrong. *Journal of Physical Chemistry C*[J], 2014, 118(11): 5626
56 Lu Xihong, Wang Gongming, Zhai Teng *et al. Nano Letters*[J], 2012, 12(3): 1690
57 Xiao Peng, Liu Dawei, Garcia B B *et al. Sensors & Actuators B: Chemical*[J], 2008, 134(2): 367
58 Jorcin J B, Orazem M E, Pébère N *et al. Electrochimica Acta*[J], 2006, 51(8): 1473

非晶TiO_2纳米管形貌对其作为超级电容器电化学性能的影响

宋致远[1]，李线绒[1]，庄昌万[1]，卫爱丽[1]，张王刚[1]，刘一鸣[1,2]

(1. 太原理工大学 材料科学与工程学院，山西 太原 030024)

(2. 山西省分析科学院，山西 太原 030006)

摘　要：采用改进的两步电化学阳极氧化和电化学氢化法制备了不同管径、长度和壁厚的氢化无定型TiO_2纳米管阵列（H@am-TNAs）。结果表明，电化学氢化对TiO_2纳米管阵列的结构影响不大。经过电化学氢化后，纳米管在100 mV·s^{-1}时的比电容为4.05 mF·cm^{-2}，比未氢化的管长和管径相同的TiO_2纳米管的比电容大20倍。纳米管的比电容不仅与管长有关，还受管径的影响。通过指数函数拟合，纳米管的长径比呈线性关系。面积电容/长径比达到0.056，几乎相当于锐钛矿相TiO_2纳米管。阳极化处理后的纳米管具有最小的电荷转移阻力和最佳的离子扩散/输运动力学，具有最高的面积容量。此外，为了研究H@am-TNAs纳米管的电化学性能的润湿性，相同的H@am-TNAs电极在*C-V*和*C-P*测试前，在电解液中浸泡不同时间，结果表明，比电容随着浸泡时间的增加而减小。

关键词：超级电容器；无定型；二氧化钛纳米管；长径比；电化学氢化

作者简介：宋致远，男，1996年生，硕士，太原理工大学材料科学与工程学院，山西 太原 030024，E-mail：songzy1212@163.com